

DFTT 03/95

DTP/95/08

Cavendish-HEP-95/14

October 1995

# $e^+e^- \rightarrow b\bar{b}W^+W^-$ events at the Next Linear Collider: colour structure of top signal and irreducible background

A. Ballestrero<sup>a</sup>, V.A. Khoze<sup>b</sup>, E. Maina<sup>a</sup>,  
S. Moretti<sup>c</sup> and W.J. Stirling<sup>b,d</sup>

*a) Dipartimento di Fisica Teorica, Università di Torino,  
and I.N.F.N., Sezione di Torino,  
Via Pietro Giuria 1, 10125 Torino, Italy.*

*b) Department of Physics, University of Durham,  
South Road, Durham DH1 3LE, United Kingdom.*

*c) Cavendish Laboratory, University of Cambridge,  
Madingley Road, Cambridge CB3 0HE, UK.*

*d) Department of Mathematical Sciences, University of Durham,  
South Road, Durham DH1 3LE, United Kingdom.*

## Abstract

We examine the colour structure and charged particle yield for both the  $t\bar{t}$  signal and the irreducible background processes contributing to  $e^+e^- \rightarrow b\bar{b}W^+W^-$  production close to the  $t\bar{t}$  threshold. The charged particle multiplicity for the various components of the cross section is computed as a function of several kinematic variables. Our study may have important implications for recently proposed studies of interconnection phenomena in  $t\bar{t}$  production at high-energy  $e^+e^-$  colliders.

## 1. Introduction

One of the most important physics topics at future  $e^+e^-$  linear colliders is the detailed study of the top quark. In particular, a unique precision in the top mass determination (with an accuracy of a few hundred MeV) is anticipated, see for example Refs. [1, 2, 3, 4]. One of the obvious requirements for the success of such precise studies is a detailed understanding of the background processes, in particular of the colour structure of the  $e^+e^- \rightarrow b\bar{b}W^+W^-$  background events.

Recall that the dominance of the  $t \rightarrow bW^+$  weak decay mode leads to a large top width  $\Gamma_t$ , which is approximately 1.6 GeV for  $m_t \simeq 180$  GeV. This width is larger than the typical hadronic scale  $\mu \sim 1$  fm $^{-1}$ , and so the top decays before it has time to hadronize [5, 6]. It is precisely this large decay width that makes top physics so unique. First, the top decay width  $\Gamma_t$  provides an infrared cut-off for the strong forces between the  $t$  and the  $\bar{t}$  [7, 8, 9]: the width acts as a physical ‘smearing’ [10], and top production becomes a quantitative prediction of perturbative QCD, largely independent of non-perturbative phenomenological algorithms. Second,  $\Gamma_t$  controls the size of QCD interferences between radiation occurring at different stages of the  $t\bar{t}$  production process [11, 12, 13]. These interferences affect the structure of the colour flows in the  $t\bar{t}$  events, and may provide a potentially serious source of uncertainty in the reconstruction of the final state.

As is discussed in detail in Ref. [14] (see also [15]), particle production in events of the type

$$e^+e^- \rightarrow t\bar{t} \rightarrow b\bar{b}W^+W^- \quad (1)$$

could depend in a non-trivial way on the kinematics of the process. The effects of *energetic* perturbative gluon radiation are suppressed because of the space-time separation between the decays of the  $t$  and  $\bar{t}$  quarks. Soft gluon emission and non-perturbative fragmentation introduce a correlation (interconnection) between the  $b$ - and  $\bar{b}$ -jets coming from the top decays. As a result, the  $b$  and  $\bar{b}$  have to ‘cross-talk’ in order to produce a final state made up of colourless hadrons<sup>1</sup>.

Such interconnection phenomena could affect the final state in  $t\bar{t}$  events in many respects. In order to quantify their size, it was proposed in Ref. [14] to examine the

---

<sup>1</sup>Analogously to Ref. [14], throughout this paper we assume for simplicity that the  $W$ ’s decay leptonically.

average multiplicity of double leptonic  $t\bar{t}$  decays as a function of the relative angle between the  $b$ - and the  $\bar{b}$ -jets. Such studies could provide important information about the size of the interconnection-related systematic uncertainties in the top mass reconstruction. They are also interesting in their own right, since they potentially open up a new laboratory for probing non-perturbative QCD dynamics, see for example Refs. [14, 15, 16, 17].

The issue of background processes was not addressed in Ref. [14]. Since the interconnection effects in the distributions of the final-state particles in the process

$$e^+e^- \rightarrow b\bar{b}W^+W^- \quad (2)$$

are comparatively weak, and since the background contributions are quite different in various kinematical regions, the detailed properties of the colour flow structure of the background events need special detailed consideration. Here we present a complete analysis of the full process (2) by studying (i) the detailed colour structure of  $t\bar{t}$  production and decay, and (ii) the colour structure of the irreducible backgrounds in  $b\bar{b}W^+W^-$  production.

This paper is organised as follows. In Section 2 we give a detailed description of the structure of the matrix element for the reaction  $e^+e^- \rightarrow b\bar{b}W^+W^-$ . Numerical results are given in Section 3 and the conclusions are presented in Section 4.

## 2. Colour Structure of the Matrix Element

The matrix element used in this study is the one already introduced in Refs. [18, 19], where further details (method of calculation, parameter values, etc.) can be found. Only the value of the Higgs mass  $M_H$  has been changed in the present work. Since in the present context we are not interested in effects due to virtual Higgs states, we deliberately increased  $M_H$  to a value greater than the collision energy, viz.  $M_H = 600$  GeV for  $\sqrt{s} \leq 500$  GeV. We use the value  $m_t = 175$  GeV for the top quark mass, as suggested by recent data [20].

With the assumption that the Higgs mass is always larger than the collider CM energy, the dominant contributions to the modulus squared of the scattering amplitude are (see Ref. [19]):

- (i) double  $t$ -resonance (i.e.  $t\bar{t} \rightarrow b\bar{b}W^+W^-$ , Fig. 1a),

- (ii) single  $t$ -resonance (i.e.  $t \rightarrow bW^+ +$  charged conjugate, Fig. 1b),
- (iii)  $Z^0$ -resonance (i.e.  $Z^0 \rightarrow b\bar{b}$ , Fig. 1c),
- (iv) non-resonant (NR) (Fig. 1d together with those in Fig. 1c involving the splitting process  $\gamma^* \rightarrow b\bar{b}$ ).

If we denote by  $M_j$  the sum of the diagrams in the  $j$ th channel, and neglect Higgs contributions, we have

$$M_{tot} = \sum_{j=1}^4 M_j, \quad (3)$$

where  $M_{tot}$  is the total Feynman amplitude. In squaring Eq. (3), we define the combinations<sup>2</sup>

$$\mathcal{M}_1 = |M_1|^2, \quad (4)$$

$$\mathcal{M}_2 = |M_2|^2 + 2\text{Re}[M_1 M_2^*] \quad (5)$$

$$\mathcal{M}_3 = |M_3|^2, \quad (6)$$

$$\mathcal{M}_4 = |M_4|^2 + \text{all remaining interference terms}, \quad (7)$$

such that

$$|M_{tot}|^2 = \sum_{j=1}^4 \mathcal{M}_j. \quad (8)$$

We associate these four combinations with the contributions (i) – (iv) defined above.

When discussing the structure of the particle flows corresponding to the background processes (ii), (iii) and (iv), it is convenient to apply the standard ‘parton shower plus fragmentation’ picture for  $e^+e^- \rightarrow \gamma^*, Z^0 \rightarrow q\bar{q}$ , various aspects of which are now well understood. Analogously to Ref. [14], the colour flow distribution can easily be described using the language of QCD antennae/dipoles (for details see [22]). Thus, the radiation pattern corresponding to the diagrams of Fig. 1c and 1d is given by the  $\hat{b}\bar{b}$  antenna which describes the production of hadrons in the process  $\gamma^*, Z^0 \rightarrow b\bar{b}$ . Because of the large amount of data from PETRA/PEP and LEP1/SLC, the properties of  $b$ -jets in this process are now well understood. A specific role is played here by kinematical

---

<sup>2</sup>Note that only the *sum* of these is positive definite. In particular, the interference terms in  $\mathcal{M}_4$  can cause the corresponding contribution to the cross section to be zero or negative, see Figs. 3 and 4 below.

configurations in which the  $b$ – and  $\bar{b}$ –jets come from the decay of an on–mass–shell  $Z^0$  boson. For these configurations the average particle multiplicity is given by the multiplicity in  $Z^0 \rightarrow b\bar{b}$ , as measured for example at LEP1. For the non–resonant processes in Fig. 1 the average multiplicity of the final–state particles depends strongly on the relative orientation of the  $b$ – and  $\bar{b}$ –jets. In contrast, for the double  $t$ –resonance (Fig. 1a) and single  $t$ –resonance (Fig. 1b) mechanisms the angular dependence is comparatively weak (but nonetheless readily visible) because of the suppressed role of the  $\hat{b}\bar{b}$  antennae [14].

It is worthwhile to mention that not far from the  $t\bar{t}$  threshold the final–state structure corresponding to double top–resonant production is dominated by two essentially azimuthally symmetric  $b$ – and  $\bar{b}$ –jets, while the background  $\gamma^*, Z^0 \rightarrow b\bar{b}$  processes are described by the  $\hat{b}\bar{b}$  antenna patterns with all the appropriate azimuthal asymmetry effects (see Ref. [22]). Moreover, the  $\gamma^* \rightarrow b\bar{b}$  contribution enhances the role of low multiplicity events. Note also that with increasing collision energy the  $b$ – and  $\bar{b}$ –jets coming from  $t\bar{t}$  production tend to be more back–to–back, while those resulting from  $\gamma^*, Z^0 \rightarrow b\bar{b}$  splitting tend to become more collinear.

### 3. Results

Our numerical results are presented in Figs. 2–8. In all of them we distinguish between the  $e^+e^- \rightarrow b\bar{b}W^+W^-$  components (i) — (iv) discussed in the previous section and in Refs. [18, 19].

In Fig. 2 we show the dependence of the various contributions on the collider centre–of–mass (CM) energy, in the range  $200 \text{ GeV} \lesssim \sqrt{s} \lesssim 500 \text{ GeV}$ . The behaviour of the various curves can be readily understood in terms of the diagrams contributing to the  $\mathcal{M}_i^2$  amplitudes, see Fig. 1. The  $t\bar{t} \rightarrow b\bar{b}W^+W^-$  curve corresponds to  $t\bar{t}$ –pair production followed by the decays  $t \rightarrow bW^+$  and  $\bar{t} \rightarrow \bar{b}W^-$ , both above ( $\sqrt{s} \geq 350 \text{ GeV}$ ) and below threshold ( $\sqrt{s} < 350 \text{ GeV}$ ). In contrast to the naive case of the ‘narrow width approximation’ (see Ref. [18]), in which this process is computed in terms of a *production*  $\times$  *decay* reaction  $\sigma(e^+e^- \rightarrow t\bar{t}) \times [BR(t \rightarrow bW)]^2$  with zero top width in the production process (top quarks produced on–shell) and independent semileptonic top decays, here both  $t$ –quark finite width effects and energy/spin correlations between

the two top decays are included. The consequence<sup>3</sup> of this is clearly visible in the dependence of the cross section on  $\sqrt{s}$ . In particular, there is a significant ‘shoulder’ which extends far below the nominal threshold.

This behaviour naturally also affects the other  $e^+e^- \rightarrow b\bar{b}W^+W^-$  contributions that include interferences with the double top resonance channel, such as  $t \rightarrow bW^+$  and NR. This is clearly visible in both of these as the little ‘bump’ around  $\sqrt{s} = 2m_t$ , which slightly decreases the cross section in the first case and enhances it in the second. It is important to stress that these curves, and therefore their interplay, have no *separate* physical meaning, since the  $\mathcal{M}_i^2$ ’s are not separately gauge invariant, but they provide a useful way of looking inside the process and distinguishing between the different interactions. The final step must always be to sum together all the various components  $\mathcal{M}_i^2$  and consider the total rates.

On their own, the curves in Fig. 2 corresponding to  $t \rightarrow bW^+$  and NR describe, respectively, the production of a single top quark through a highly virtual  $W^{\pm*}$  decaying to  $tb$  pairs with  $t \rightarrow bW$ , and dominantly (as will be apparent from Figs. 3–4, see below) of a  $b\bar{b}$ –pair from  $\gamma^* \rightarrow b\bar{b}$ . In the first case the main contribution to single top production comes from diagrams in which the decaying  $W^\pm$  is produced via  $t$ –channel exchange (i.e. the second diagram of Fig. 1b) rather than via  $s$ –channel exchange (i.e. the first and third diagrams of Fig. 1b), since the corresponding curve in Fig. 2 does not show any decrease with  $\sqrt{s}$  above the nominal threshold at  $m_t + M_W + m_b \approx 260$  GeV. In the second case, except for the range  $270 \text{ GeV} \lesssim \sqrt{s} \lesssim 360 \text{ GeV}$  where the interferences between non–resonant and resonant diagrams are important, the shape is almost flat, reflecting the dominance of the  $t$ –channel contribution (the first, second and fifth diagrams of Fig. 1c, with a  $\gamma$  propagator) to  $\gamma^*W^+W^-$  production followed by the  $\gamma^* \rightarrow b\bar{b}$  splitting. Finally, the curve corresponding to the  $Z^0 \rightarrow b\bar{b}$  background illustrates the characteristic features of the production of three vector

---

<sup>3</sup>Other effects are discussed in Ref. [18]. Note that analogously to Ref. [18] we do not address here the issue of the QCD Coulomb attraction effects in process (1). These effects are especially important near the  $t\bar{t}$  threshold where they substantially enhance the production amplitude. The Coulomb physics could be incorporated using the technique of non–relativistic Green’s functions for the  $t\bar{t}$  system [7, 8] which has now become quite routine, see Refs. [1, 2, 3, 4] and references therein. The background amplitudes which are our main concern in this paper are only weakly affected by QCD final–state interactions. We should also mention that in the present study we do not take into account QED Initial State Radiation (ISR), but these effects would be straightforward to include.

bosons  $Z^0W^+W^-$ , with the  $Z^0$  decaying to the  $b\bar{b}$ -pair, with a threshold at  $2M_W + M_Z \approx 250$  GeV and a dominant  $t$ -channel exchange structure (the first, second and fifth diagrams of Fig. 1c, with a  $Z^0$ -propagator).

As already mentioned, we concentrate on the case of leptonic decays of *both* the  $W^\pm$ 's. This implies that we have final states with two neutrinos and therefore with missing energy and transverse momentum:  $b\bar{b}W^+W^- \rightarrow b\bar{b}(\ell\nu_\ell)(\ell'\nu_{\ell'})$  or more generally  $jjW^+W^- \rightarrow jj(\ell\nu_\ell)(\ell'\nu_{\ell'})$ , depending on whether or not one can exploit the possibility of using  $b$ -tagging [21]. This missing energy and transverse momentum prevents us from studying the kinematics of  $e^+e^- \rightarrow b\bar{b}W^+W^-$  events by looking at variables which require the reconstruction of the  $W^\pm$ 's through their decay products, for example the invariant masses  $M_{bW}$  or energies  $E_{bW}$ . These quantities would of course be extremely useful in distinguishing the  $t\bar{t}$  signal from the other  $e^+e^- \rightarrow b\bar{b}W^+W^-$  background contributions [18, 19]. Thus in the figures which follow we restrict our attention to variables involving the  $b\bar{b}$ -system only.

In Fig. 3 we show the dependence of the four components (i)–(iv) on the cosine of the angle between the  $b$  and  $\bar{b}$ , at  $\sqrt{s} = 360$  GeV. The convenience of this variable has been explained above (see also Ref. [14]). For double and single top production the angular dependence is weak, reflecting the absence of any strong correlation between the top and anti-top decay products near threshold. In contrast, the  $Z^0 \rightarrow b\bar{b}$  and NR components exhibit a more pronounced structure. For the former, we note that there is a significant boost to the  $Z^0$  at this centre-of-mass energy (note that  $\sqrt{s} = 360$  GeV is 110 GeV above the  $Z^0W^+W^-$  threshold), and so the peak at  $\cos(b\bar{b}) = -1$  corresponding to back-to-back production in the  $Z^0$  rest frame is significantly smeared out. For the NR component, the main feature is the  $\gamma^* \rightarrow b\bar{b}$  contribution which prefers small invariant masses and therefore has  $\cos(b\bar{b}) \approx 1$ .

In Figs. 4 and 5 we show the dependence of the four components on the invariant mass of the  $b\bar{b}$ -system and on the energy of the  $b(\bar{b})$  respectively. As expected, for the former we can clearly recognize both the  $M_{b\bar{b}} \approx M_Z$  peak in the  $Z^0 \rightarrow b\bar{b}$  component and the  $\gamma^* \rightarrow b\bar{b}$  contribution at small  $M_{b\bar{b}}$  in NR. Neither the double top nor the single top channel show any particularly distinctive features. Fig. 5 indicates the average energy of the  $b$ 's coming from the various subprocesses: approximately 70 GeV for  $t\bar{t} \rightarrow b\bar{b}W^+W^-$ , 80 GeV for  $t\bar{b}W^+$  and 60 GeV for  $Z^0 \rightarrow b\bar{b}$ . For the NR component there is a preference for small  $b$  energies.

We next adopt a semi-qualitative procedure for evaluating the average charged multiplicities corresponding to the different contributions to the  $e^+e^- \rightarrow b\bar{b}W^+W^-$  events not far from the  $t\bar{t}$  threshold. This procedure is based on the antenna pattern analysis [11, 12, 13] of soft gluon radiation in top quark production events within the framework of the MLLA-LPHD picture of multiple hadron production [22].

Our starting point is the multiplicity  $N_{b\bar{b}}(W)$  in  $e^+e^- \rightarrow b\bar{b}$  production at CM energy  $W = \sqrt{s} = 2E_b$ , where  $E_b$  is the energy of the  $b$ -jet in the CM system. According to the MLLA-LPHD scenario (see Ref. [23] for details)  $N_{b\bar{b}}$  can be expressed in terms of the multiplicity  $N_{q\bar{q}}$  in the light-quark production process  $e^+e^- \rightarrow q\bar{q}$  as

$$N_{b\bar{b}}(W) = N_{q\bar{q}}(W) + \delta_b, \quad (9)$$

where the difference  $\delta_b$  is  $W$ -independent. This prediction of perturbative QCD is in a good agreement with existing experimental data [24], from which one obtains  $\delta_b \simeq 3$ . For  $N_{q\bar{q}}(W)$  one can use the MLLA-inspired simple analytical formula proposed in Ref. [25]. As a result, the charged particle multiplicity in  $b\bar{b}$  events can be readily evaluated as<sup>4</sup>

$$N_{b\bar{b}}^{Z^0,\text{NR}}(E_{b(\bar{b})}, \cos(b\bar{b})) \equiv N_{b\bar{b}}^{Z^0,\text{NR}}(M_{b\bar{b}}) \approx 5.85 + 0.125 \exp[2.317 \sqrt{\log(M_{b\bar{b}}/\text{GeV})}], \quad (10)$$

with<sup>5</sup>  $M_{b\bar{b}}^2 = 2(E_b E_{\bar{b}} - |p_b||p_{\bar{b}}| \cos(b\bar{b}) + m_b^2)$  and  $|p_{b(\bar{b})}|^2 = E_{b(\bar{b})}^2 - m_b^2$ .

Motivated by the results of Refs. [11, 12, 13] we can approximate the average multiplicities corresponding to the  $t$ -resonant production processes ((i) and (ii)) by

$$N_{b\bar{b}}^{t\bar{t},t}(E_{b(\bar{b})}, \cos(b\bar{b})) \equiv N_{b\bar{b}}^{t\bar{t},t}(E_b, E_{\bar{b}}) \approx \frac{1}{2} N_{b\bar{b}}^{Z^0,\text{NR}}(M_{b\bar{b}} \rightarrow 2E_b) + \frac{1}{2} N_{b\bar{b}}^{Z^0,\text{NR}}(M_{b\bar{b}} \rightarrow 2E_{\bar{b}}), \quad (11)$$

where  $E_b$  and  $E_{\bar{b}}$  are the actual CM energies of the  $b$ - and  $\bar{b}$ -jets, respectively. This result accounts for the contributions of the antennae of the type  $\hat{t}b$ ,  $\hat{\bar{t}}\bar{b}$  or  $\hat{t}\bar{b}$ ,  $\hat{\bar{t}}b$  (note that interconnection effects are not included here).

---

<sup>4</sup>Of course one could alternatively apply all the powerful machinery of the successful Monte Carlo algorithms (JETSET, HERWIG, ARIADNE). However for the purposes of this paper we can safely restrict ourselves to the estimates based on Eq. (10). It is remarkable that in a wide energy domain the predictions of Eq. (10) are in a very good agreement with the results of the JETSET parton shower Monte Carlo program [26]. (We are grateful to T. Sjöstrand for providing us with the numerical results of JETSET for  $N_{b\bar{b}}(W)$ ).

<sup>5</sup>The superscripts  $t\bar{t}$ ,  $t$ ,  $Z^0$  and NR in Eqs. (10,11) refer to the production mechanisms (i)–(iv) of the  $b\bar{b}$ -pair in  $e^+e^- \rightarrow b\bar{b}W^+W^-$  events.

Using the above formulae (i.e. Eq. (10) for the multiplicity for the  $Z^0 \rightarrow b\bar{b}$  and the non-resonant contributions ((iii) and (iv)) and Eq. (11) for the double and single  $t$ -resonant contributions ((i) and (ii)), we can study the quantities

$$\langle N_{\cos}^i \rangle = \frac{\int dE_{b(\bar{b})} \mathcal{I}^i(E_{b(\bar{b})}, \cos(b\bar{b}))}{\int dE_{b(\bar{b})} \mathcal{J}^i(E_{b(\bar{b})}, \cos(b\bar{b}))}, \quad (12)$$

$$\langle N_E^i \rangle = \frac{\int d\cos(b\bar{b}) \mathcal{I}^i(E_{b(\bar{b})}, \cos(b\bar{b}))}{\int d\cos(b\bar{b}) \mathcal{J}^i(E_{b(\bar{b})}, \cos(b\bar{b}))}, \quad (13)$$

at fixed CM energy ( $\sqrt{s} = 360$  GeV), and

$$\langle N_{\text{tot}}^i \rangle = \frac{\int dE_{b(\bar{b})} d\cos(b\bar{b}) \mathcal{I}^i(E_{b(\bar{b})}, \cos(b\bar{b}))}{\int dE_{b(\bar{b})} d\cos(b\bar{b}) \mathcal{J}^i(E_{b(\bar{b})}, \cos(b\bar{b}))}, \quad (14)$$

as a function of the CM energy in the range 240–390 GeV, with  $i = t\bar{t}, t, Z^0$  and NR. In Eqs. (12)–(14)  $\mathcal{I}^i$  and  $\mathcal{J}^i$  are given by

$$\mathcal{I}^i(E_{b(\bar{b})}, \cos(b\bar{b})) = \frac{d\sigma^i}{dE_{b(\bar{b})} d\cos(b\bar{b})} N_{b\bar{b}}^i(E_{b(\bar{b})}, \cos(b\bar{b})), \quad (15)$$

and

$$\mathcal{J}^i(E_{b(\bar{b})}, \cos(b\bar{b})) = \frac{d\sigma^i}{dE_{b(\bar{b})} d\cos(b\bar{b})}, \quad (16)$$

where  $\sigma^i$  is the total ‘cross section’ of the  $i$ -th component.

The above quantities can be interpreted as the average number of charged particles per unit interval of the cosine of the angle between the  $b$ - and  $\bar{b}$ -jets (Eq. (12)) and per unit interval of the energy of the  $b(\bar{b})$ -jets (Eq. (13)), and as the total number of charged particles for all  $\cos(b\bar{b})$  angles and  $E(b)$  energies (Eq. (14)). These are defined for each of the four components (i)–(iv) separately. The distributions for  $\langle N_{\cos}^i \rangle$ ,  $\langle N_E^i \rangle$  and  $\langle N_{\text{tot}}^i \rangle$  are plotted in Figs. 6, 7 and 8, respectively<sup>6</sup>.

In Fig. 6 the multiplicity arising from the double and single  $t$ -resonant contributions is essentially independent of the angle between the  $b$ -jets. This follows from the fact that (i) the multiplicity here (Eq. (11)) does not depend explicitly on the angle, and (ii) the distribution of the energy of the  $b$ -quarks (Fig. 4) is rather sharply peaked in both cases around 60–80 GeV. The multiplicity from the  $Z^0 \rightarrow b\bar{b}$  contribution is also approximately independent of the angle (reflecting the fact that  $M_{b\bar{b}} \approx M_Z$  is

---

<sup>6</sup>Note that in Figs. 6–8 a cut on the energy of the  $b$ - and  $\bar{b}$ -jets has been applied, i.e.  $E(b, \bar{b}) > 20$  GeV.

constant) apart from near  $\cos(b\bar{b}) = 1$  where  $M_{b\bar{b}} < M_Z$ . In this region, however, the corresponding cross section is very small, see Fig. 3. The non-resonant contribution decreases steadily as  $\cos(b\bar{b})$  increases as the  $\gamma^* \rightarrow b\bar{b}$  contribution (which prefers small  $M_{b\bar{b}}$  and hence smaller multiplicity) becomes more important.

In Fig. 7 the multiplicity arising from the double and single  $t$ -resonant contributions rises smoothly with increasing  $E_b$ , as expected from Eq. (11). The slight fall off at very large  $E_b$  (where the cross section is very small, see Fig. 5) is caused by asymmetric configurations where  $E_b \gg E_{\bar{b}}$  or *vice versa*. The multiplicity from the  $Z^0 \rightarrow b\bar{b}$  contribution is essentially constant over the whole energy range and the non-resonant contribution multiplicity increases quite sharply with  $E_b$ , reflecting the underlying dependence on  $M_{b\bar{b}}$ .

The collider energy dependence of the multiplicities arising from the various contributions is shown in Fig. 8. The double and single  $t$ -resonant contributions increase approximately linearly with  $\sqrt{s}$ , reflecting the underlying increase in the energy of the  $b$ -quarks. The  $Z^0 \rightarrow b\bar{b}$  contribution is approximately independent of  $\sqrt{s}$  above the threshold at  $2M_W + M_Z \approx 250$  GeV for producing on-shell  $Z^0$  bosons. The non-resonant multiplicity is somewhat smaller, reflecting the on-average smaller values of  $M_{b\bar{b}}$ , and increases slowly with  $\sqrt{s}$ . Also shown (continuous line) in Fig. 8 is the sum over the four components, obtained using the formula

$$\langle N_{\text{tot}}^{\text{sum}} \rangle = \frac{\sum_i \langle N_{\text{tot}}^i \rangle \sigma^i}{\sum_i \sigma^i}, \quad (17)$$

where  $i$  refers as usual to the contributions  $t\bar{t} \rightarrow b\bar{b}W^+W^-$ ,  $t \rightarrow bW^+ +$  charged conjugate,  $Z^0 \rightarrow b\bar{b}$  and non-resonant. This total multiplicity simply interpolates between the non-resonant contribution, which dominates the total cross section for  $\sqrt{s} \lesssim 250$  GeV, and the double-resonant  $t\bar{t}$  contribution, which dominates the total cross section from just below the  $t\bar{t}$  threshold, see Fig. 2.

## 4. Conclusions

A high-energy  $e^+e^-$  collider would provide the ideal laboratory for precision top-quark physics. Whether one considers an accurate measurement of the top-quark mass or a detailed study of the non-perturbative QCD dynamics and interconnection effects associated with  $t\bar{t}$  production, one certainly needs a more detailed understanding of

the colour structure of the background events in order to separate their influence from the subtle interference phenomena in the top signal.

In this paper we have examined the colour structure and charged particle yield in both the  $t\bar{t}$  signal and background processes contributing to  $e^+e^- \rightarrow b\bar{b}W^+W^-$  production not far from the  $t\bar{t}$  threshold. Since the relative contribution of the background processes to the total particle yield in  $e^+e^- \rightarrow b\bar{b}W^+W^-$  events is relatively small (see Fig. 2), we have been able to use an approximate procedure for evaluating the charged particle multiplicities.

Figures 6–8 contain the main results of our study. They show the multiplicities associated with the various resonant and non-resonant components of the cross section, as functions of the energies of the  $b$ - and  $\bar{b}$ -jets, the angle between them, and the overall collider energy. The colour structure of the various components is very different (see Fig. 1) and this is reflected in the multiplicity distributions. It is important, therefore, that the background contributions are carefully taken into account in studies of interconnection phenomena in  $t\bar{t}$  production.

## Acknowledgements

We thank T. Sjöstrand for valuable discussions. This work is supported in part by the Ministero dell’ Università e della Ricerca Scientifica, the UK PPARC, and the EC Programme “Human Capital and Mobility”, Network “Physics at High Energy Colliders”, contract CHRX-CT93-0357 (DG 12 COMA).

## References

- [1] Proc. of the Workshop “*Physics and Experiments with Linear Colliders*”, Saariselkä, Finland, 9–14 September 1991, eds. R. Orava, P. Eerola and M. Nordberg (World Scientific Publishing, Singapore, 1992).
- [2] Proc. of the Workshop “ *$e^+e^-$  Collisions at 500 GeV. The Physics Potential*”, Munich, Annecy, Hamburg, ed. P.M. Zerwas, DESY 92-123 A/B/C, 1992–1993.
- [3] Physics and Experiments with Linear  $e^+e^-$  colliders, eds. F.A. Harris, S.L. Olsen, S. Pakvasa and X. Tata (World Scientific Publishing, Singapore, 1993).

- [4] Proc. of the ECFA workshop on “ $e^+e^-$  Linear Colliders LC92”, ed. R. Settles, Garmisch Partenkirchen, July–August 1992, MPI-PhE/93–14, ECFA 93–154 (1993).
- [5] J.H. Kühn, *Acta Phys. Aust. Suppl.* **24** (1982) 203.
- [6] I.I. Bigi, Yu.L. Dokshitzer, V.A. Khoze, J.H. Kühn and P. Zerwas, *Phys. Lett.* **B181** (1986) 157.
- [7] V.S. Fadin and V.A. Khoze, *JETP Lett.* **46** (1987) 525; *Sov. J. Nucl. Phys.* **48** (1988) 309; *ibidem* **53** (1991) 692.
- [8] V.S. Fadin, V.A. Khoze, Proc. of the 24th LNPI Winter School, Leningrad, Vol. 1, p. 3, 1989.
- [9] V.S. Fadin, V.A. Khoze and T. Sjöstrand, *Z. Phys.* **C48** (1990) 613.
- [10] E.C. Poggio, H.R. Quinn and S. Weinberg, *Phys. Rev.* **D13** (1976) 1958.
- [11] V.A. Khoze, L.H. Orr and W.J. Stirling, *Nucl. Phys.* **B378** (1992) 413.
- [12] Yu.L. Dokshitzer, V.A. Khoze, L.H. Orr and W.J. Stirling, *Nucl. Phys.* **B403** (1993) 65.
- [13] V.A. Khoze, J. Ohnemus and W.J. Stirling, *Phys. Rev.* **D78** (1994) 1237.
- [14] V.A. Khoze and T. Sjöstrand, *Phys. Lett.* **B328** (1994) 466.
- [15] V.A. Khoze, *Durham University preprint* DTP/94/114, November 1994.
- [16] G. Gustafson, U. Pettersson and P. Zerwas, *Phys. Lett.* **B209** (1988) 90.
- [17] T. Sjöstrand and P. Zerwas, in Ref. [2], Part A, p. 463.
- [18] A. Ballestrero, E. Maina and S. Moretti, *Phys. Lett.* **B333** (1994) 434.
- [19] A. Ballestrero, E. Maina and S. Moretti, *Phys. Lett.* **B335** (1994) 460.
- [20] CDF collaboration: F. Abe *et al.*, *Phys. Rev. Lett.* **74** (1995) 2626; D0 Collaboration, *Phys. Rev. Lett.* **74** (1995) 2632.

- [21] H. Borner and P. Grosse-Wiesmann, in Ref. [2].
- [22] Yu.L. Dokshitzer, V.A. Khoze, A.H. Mueller and S.I. Troyan, *Rev. Mod. Phys.* **60** (1988) 373;  
Yu.L. Dokshitzer, V.A. Khoze, A.H. Mueller and S.I. Troyan, ‘Basics of perturbative QCD’, ed. J. Tran Thanh Van (Editions Frontiers, Gif-sur-Yvette, 1991).
- [23] V.S. Fadin, Yu.L. Dokshitzer and V.A. Khoze, *Phys. Lett.* **B115** (1982) 242; *Zeit. Phys.* **C15** (1982) 325;  
B.A. Schumm, Yu.L. Dokshitzer, V.A. Khoze and D.S. Koetke, *Phys. Rev. Lett.* **69** (1992) 3025;  
V.A. Khoze, *Durham University preprint* DTP/93/78, September 1993.
- [24] MARK II collaboration, *Phys. Rev.* **D46** (1992) 453;  
SLD collaboration, *Phys. Rev. Lett.* **72** (1994) 3145;  
OPAL collaboration, *Z. Phys.* **C61** (1994) 209;  
DELPHI collaboration, *Phys. Lett.* **B347** (1995) 447.
- [25] D.S. Koetke, *Ph.D. Thesis*, SLAC Report, SLAC-396 (1992).
- [26] T. Sjöstrand and M. Bengtsson, *Comp. Phys. Comm.* **43** (1987) 637;  
H.-U. Bengtsson and T. Sjöstrand, *Comp. Phys. Comm.* **46** (1987) 43;  
T. Sjöstrand, *CERN preprint* CERN-TH.6488/92, May 1992.

## Figure Captions

- [1] Typical Feynman diagrams describing at tree-level the four  $e^+e^- \rightarrow b\bar{b}W^+W^-$  components: (i) double  $t$ -resonance (a), (ii) single  $t$ -resonance (b), (iii)  $Z^0$ -resonance (c, with  $Z^0$ -propagators), and (iv) no resonance (c, with  $\gamma$ -propagators, and d). Internal wavy lines represent  $\gamma$ ,  $Z^0$  or  $W^\pm$ , as appropriate. Permutations of  $(W^+, W^-, \gamma^*/Z^{0*})$  and  $(\gamma^*, Z^{0*})$  along the fermion lines, exchanges between  $W^+ \leftrightarrow W^-$  in graphs involving three-vector-vertices, as well as the charged conjugate diagrams of (b) are not shown.
- [2] Dependence of the individual “total” cross sections  $\sigma_i$  on the collider energy  $\sqrt{s}$  for the four  $e^+e^- \rightarrow b\bar{b}W^+W^-$  components: (i) double  $t$ -resonance (continuous line), (ii) single  $t$ -resonance (dashed line), (iii)  $Z^0$ -resonance (dotted line), and (iv) no resonance (chain-dashed line), for  $m_t = 175$  GeV and  $M_H = 600$  GeV.
- [3] Differential distributions  $d\sigma_i/d\cos(b\bar{b})$  in the cosine of the angle between the  $b$  and  $\bar{b}$  quarks for the four  $e^+e^- \rightarrow b\bar{b}W^+W^-$  components: (i) double  $t$ -resonance (continuous line), (ii) single  $t$ -resonance (dashed line), (iii)  $Z^0$ -resonance (dotted line), and (iv) no resonance (chain-dashed line), at  $\sqrt{s} = 360$  GeV, for  $m_t = 175$  GeV and  $M_H = 600$  GeV.
- [4] Differential distributions  $d\sigma_i/dM(b\bar{b})$  in the invariant mass of the  $b\bar{b}$ -pair for the four  $e^+e^- \rightarrow b\bar{b}W^+W^-$  components: (i) double  $t$ -resonance (continuous line), (ii) single  $t$ -resonance (dashed line), (iii)  $Z^0$ -resonance (dotted line), and (iv) no resonance (chain-dashed line), at  $\sqrt{s} = 360$  GeV, for  $m_t = 175$  GeV and  $M_H = 600$  GeV.
- [5] Differential distributions  $d\sigma_i/dE(b)$  in the energy of the  $b(\bar{b})$  quark for the four  $e^+e^- \rightarrow b\bar{b}W^+W^-$  components: (i) double  $t$ -resonance (continuous line), (ii) single  $t$ -resonance (dashed line), (iii)  $Z^0$ -resonance (dotted line), and (iv) no resonance (chain-dashed line), at  $\sqrt{s} = 360$  GeV, for  $m_t = 175$  GeV and  $M_H = 600$  GeV.
- [6] Dependence of  $\langle N_{cos} \rangle$ , defined in the text, on the cosine of the angle between the  $b$  and  $\bar{b}$  quarks for the four  $e^+e^- \rightarrow b\bar{b}W^+W^-$  components: (i) double  $t$ -resonance (continuous line), (ii) single  $t$ -resonance (dashed line), (iii)  $Z^0$ -resonance (dotted

line), and (iv) no resonance (chain-dashed line), at  $\sqrt{s} = 360$  GeV, for  $m_t = 175$  GeV and  $M_H = 600$  GeV, after imposing the cut  $E(b, \bar{b}) > 20$  GeV on the energy of the  $b$ 's.

- [7] Dependence of  $\langle N_E \rangle$ , defined in the text, on the energy of the  $b(\bar{b})$  for the four  $e^+e^- \rightarrow b\bar{b}W^+W^-$  components: (i) double  $t$ -resonance (continuous line), (ii) single  $t$ -resonance (dashed line), (iii)  $Z^0$ -resonance (dotted line), and (iv) no resonance (chain-dashed line), at  $\sqrt{s} = 360$  GeV, for  $m_t = 175$  GeV and  $M_H = 600$  GeV, after the cut  $E(b, \bar{b}) > 20$  GeV on the energy of the  $b$ 's.
- [8] Dependence of  $\langle N_{\text{tot}} \rangle$ , defined in the text, on the collider energy  $\sqrt{s}$  for the four  $e^+e^- \rightarrow b\bar{b}W^+W^-$  components: (i) double  $t$ -resonance (continuous line), (ii) single  $t$ -resonance (dashed line), (iii)  $Z^0$ -resonance (dotted line), and (iv) no resonance (chain-dashed line), and for their sum (see Eq. (17)), for  $m_t = 175$  GeV and  $M_H = 600$  GeV, after imposing the cut  $E(b, \bar{b}) > 20$  GeV on the energy of the  $b$ 's.

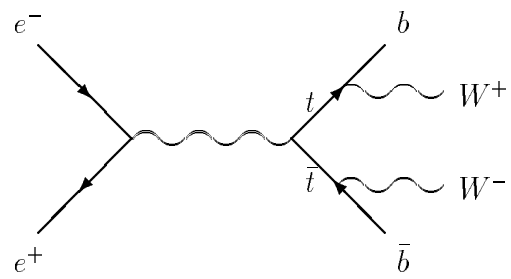


Fig. 1a

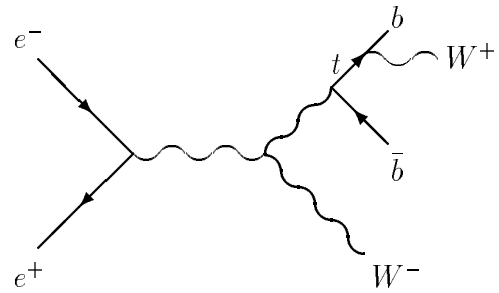
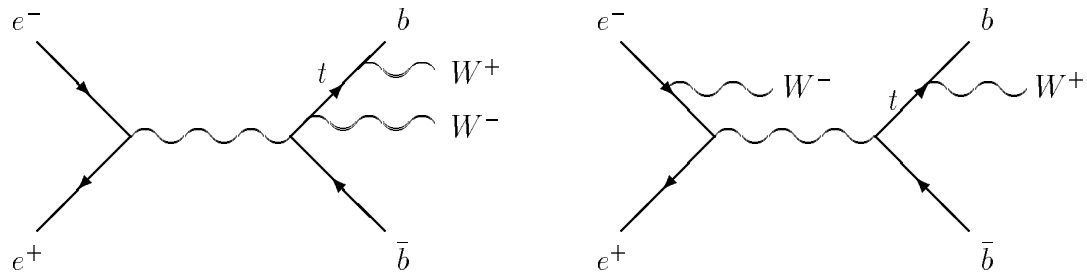


Fig. 1b

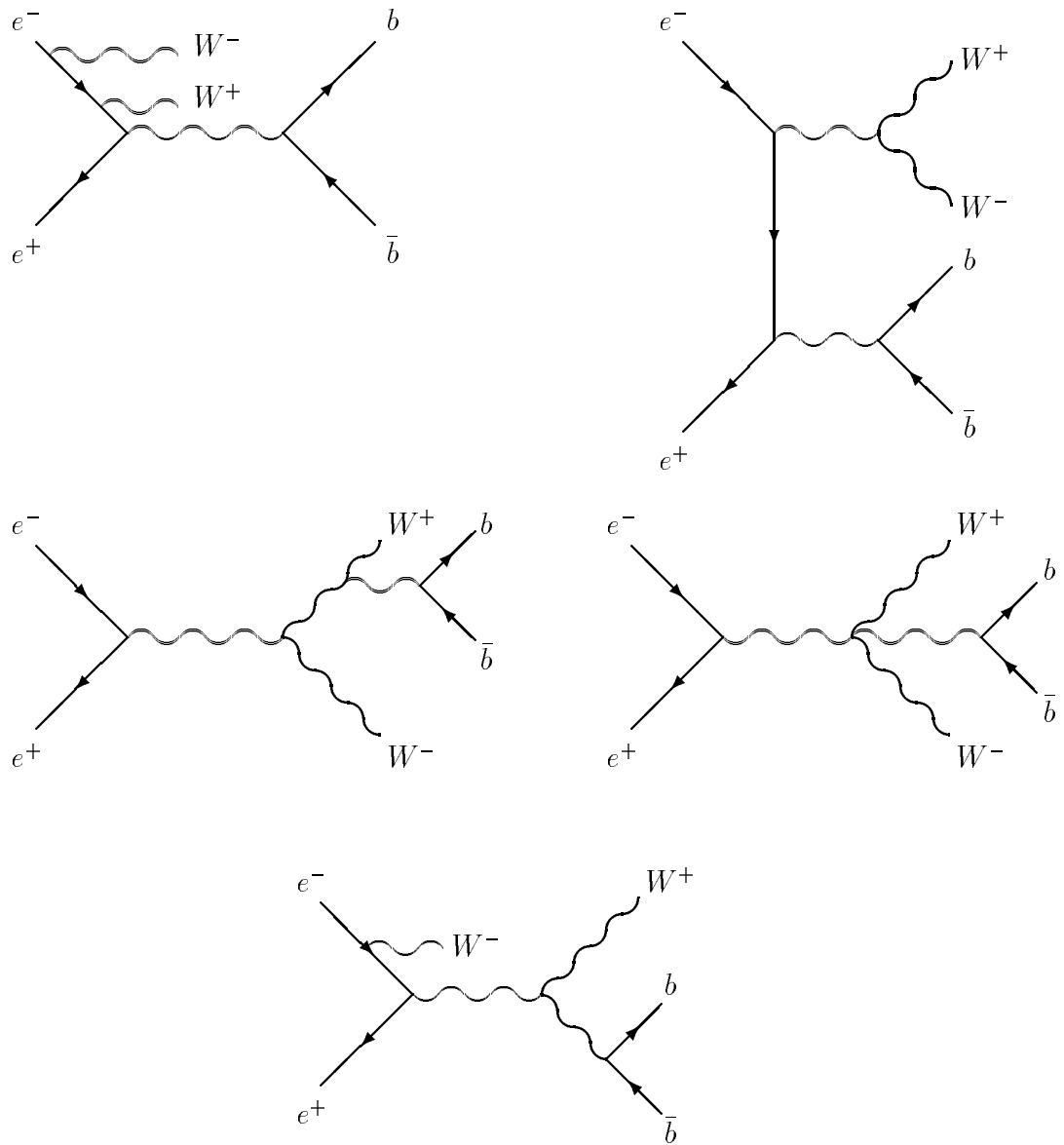


Fig. 1c

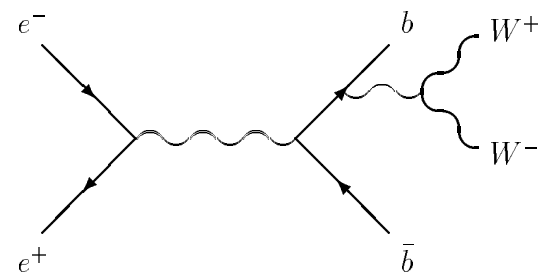


Fig. 1d

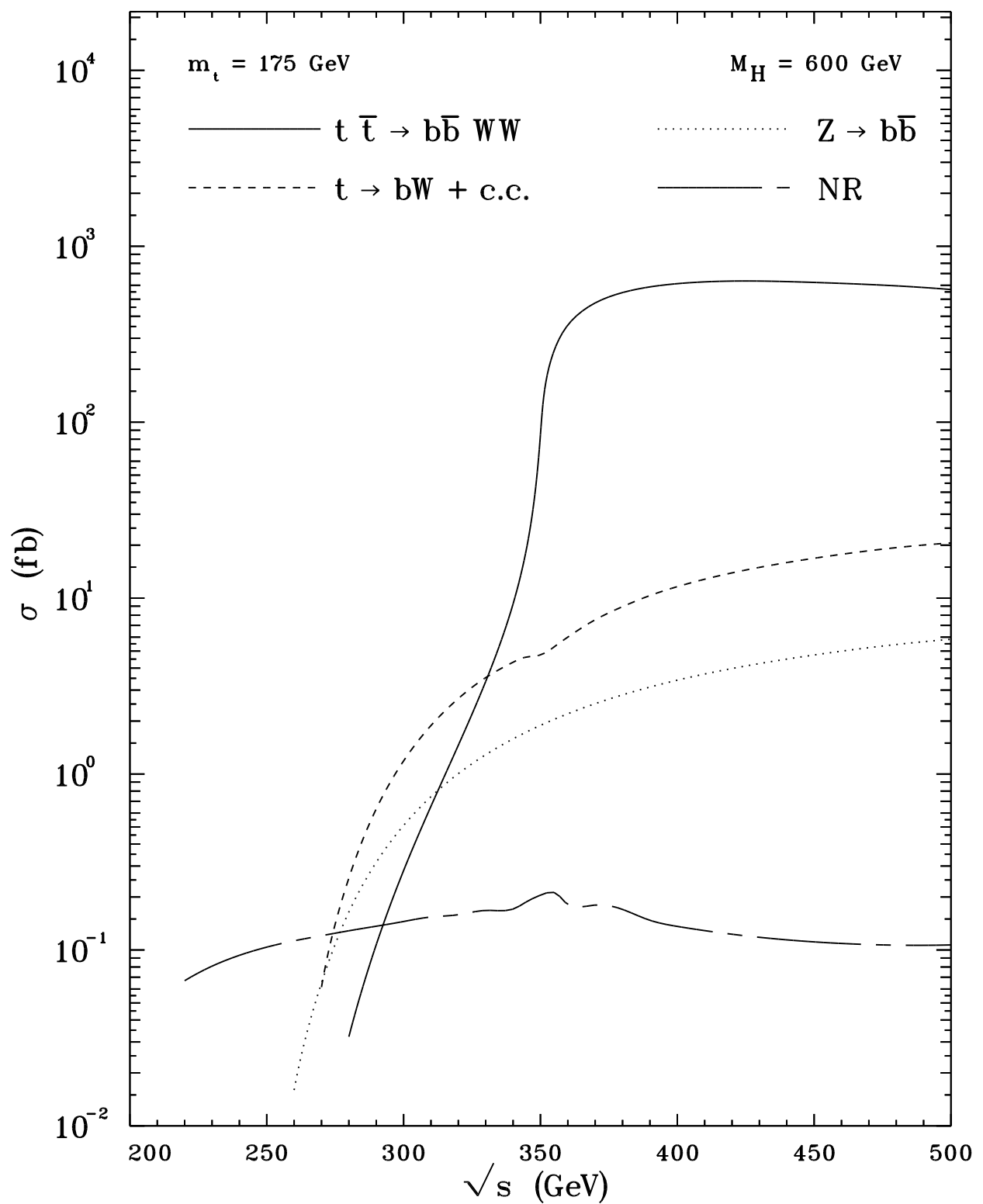


Fig. 2

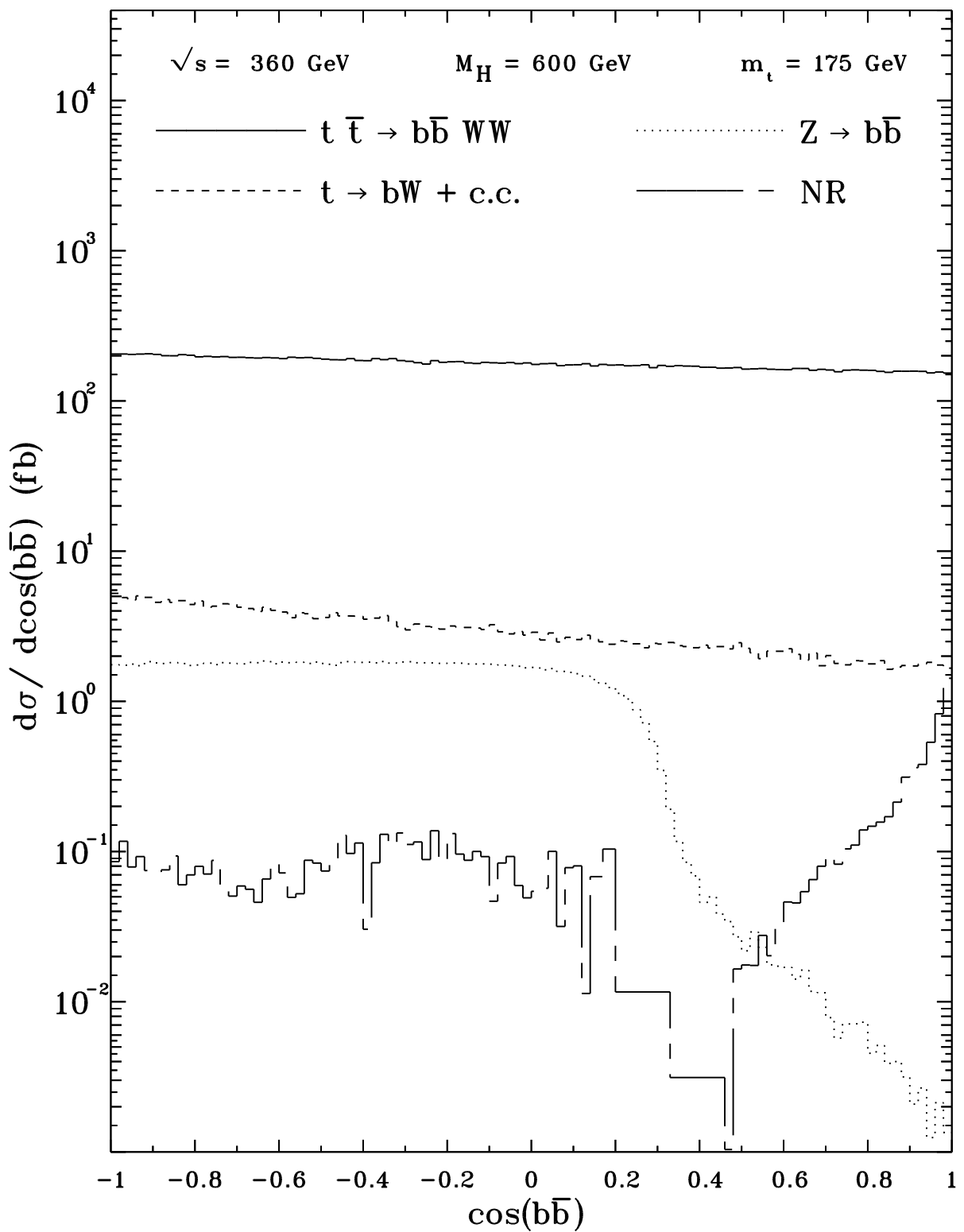
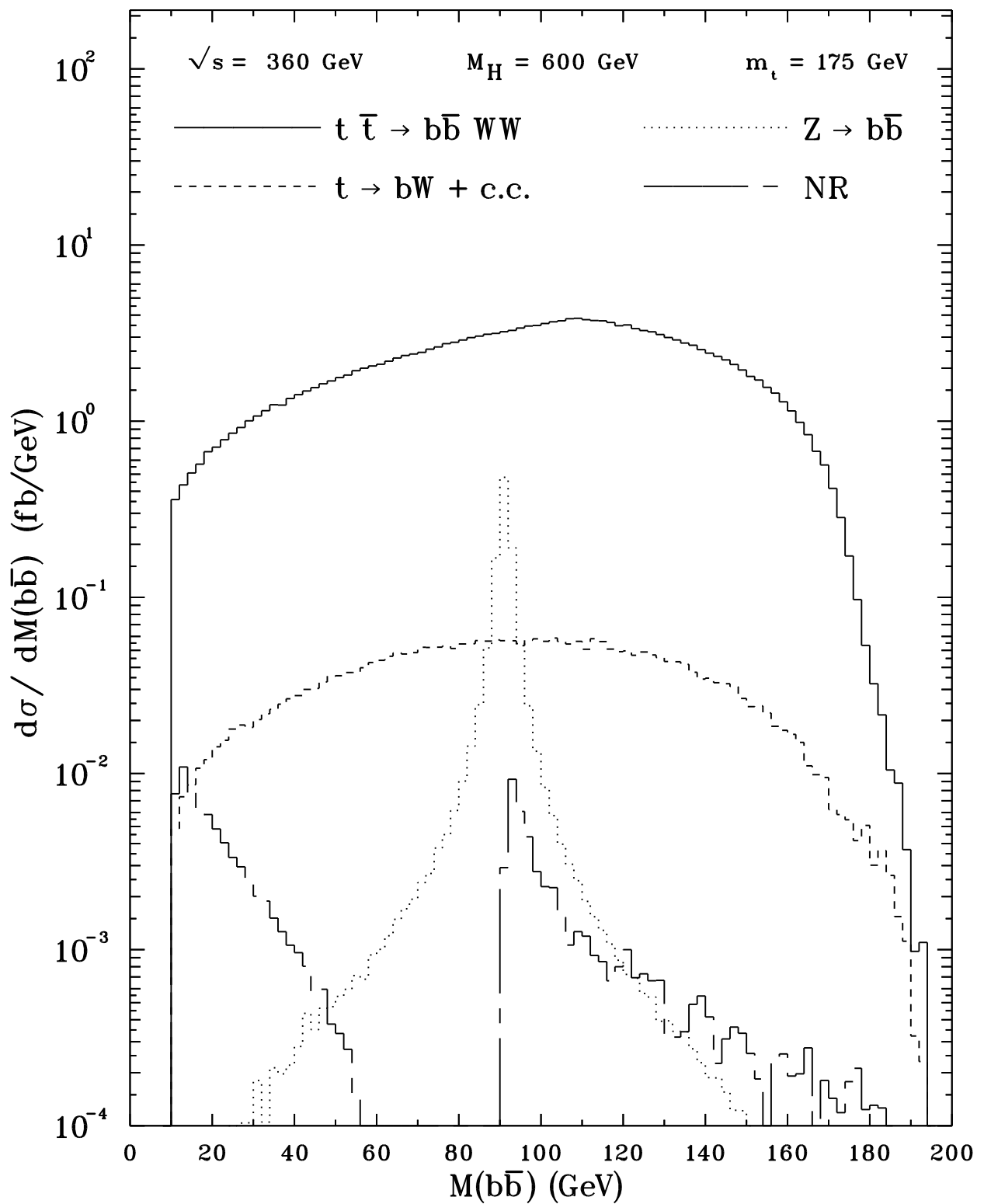


Fig. 3



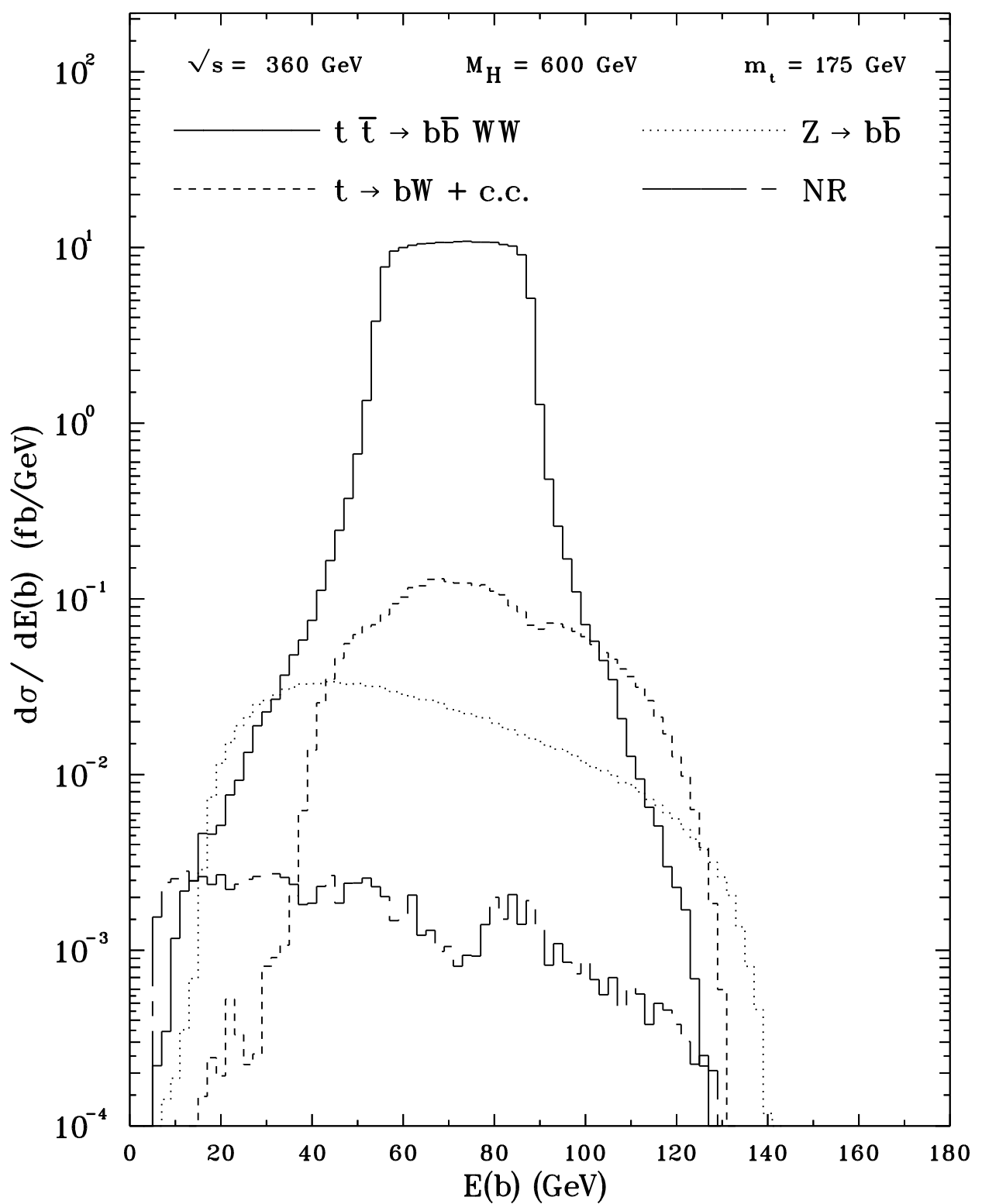


Fig. 5

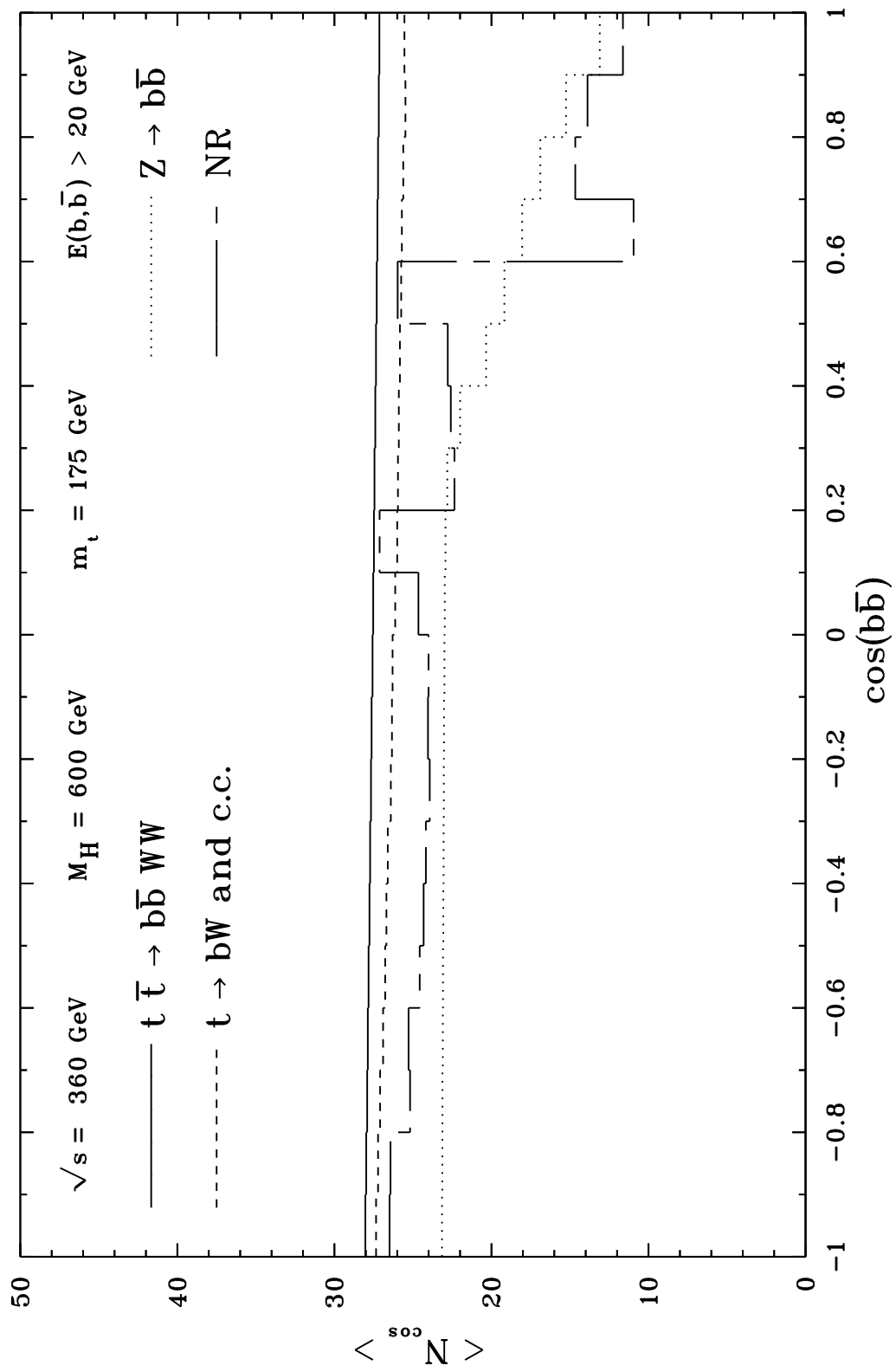


Fig. 6

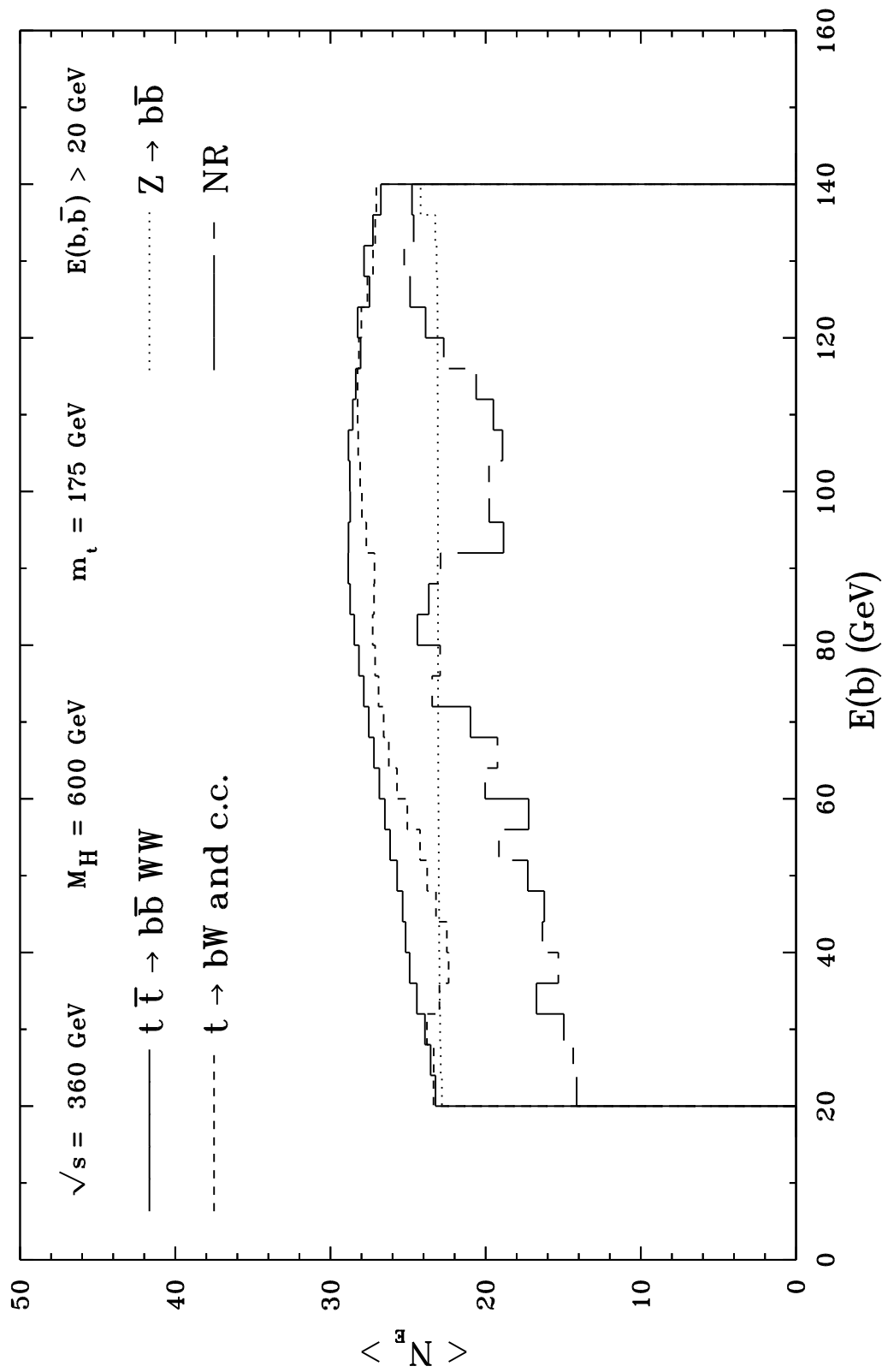


Fig.

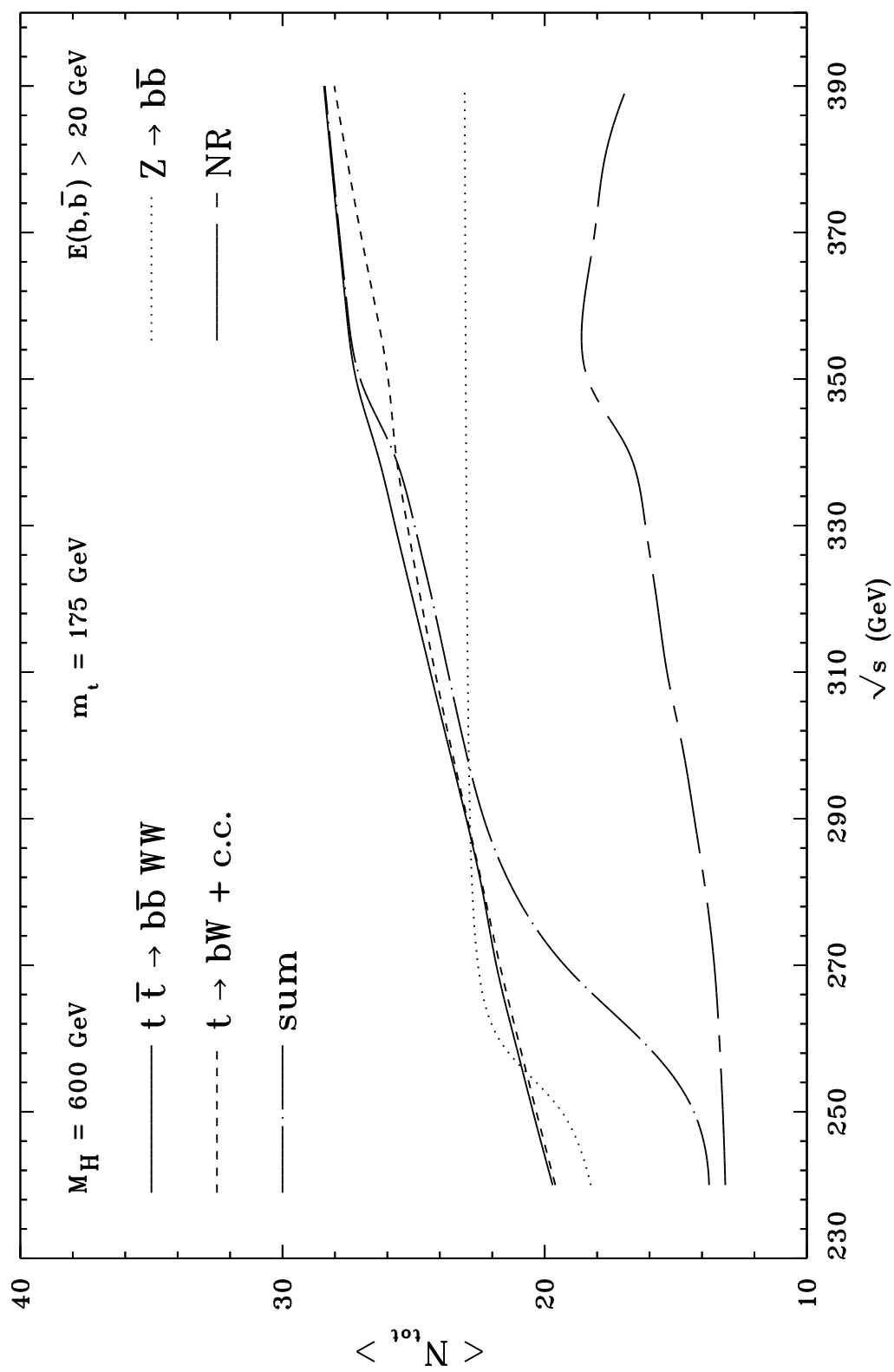


Fig. 8